








RESEARCH ARTICLE

Rheology of a sodium-molybdenum borosilicate melt undergoing phase separation

Luiz Pereira¹  | Sophie Schuller²  | Fabian B. Wadsworth³  |
 Jérémie Vasseur¹  | Ricardo F. Lancelotti⁴  | Kai-Uwe Hess¹ |
 Stéphane Gossé⁵  | Donald B. Dingwell¹ 

¹Department of Earth and Environmental Sciences,

Ludwig-Maximilians-Universität München, Munich, Germany

²CEA, DES, ISEC, DPME, University of Montpellier, Marcoule, France

³Department of Earth Sciences, Durham University, Durham, UK

⁴Department of Materials Engineering (DEMa), Federal University of São Carlos (UFSCar), São Carlos, São Paulo, Brazil

⁵Université Paris-Saclay, CEA, Service de Recherche en Corrosion et Comportement des Matériaux, Gif-sur-Yvette, France

Correspondence

Luiz Pereira, Department of Earth and Environmental Sciences, Ludwig-Maximilians-Universität München, Munich, Germany.
 Email:

luiz.pereira@min.uni-muenchen.de

Funding information

European Research Council (ERC) 2018 ADV, Grant/Award Number: 834225; São Paulo Research Foundation (FAPESP), Grant/Award Number: 2021/03374–5; Alexander von Humboldt Foundation; Orano; Électricité de France (EDF); Commissariat à l'énergie atomique et aux énergies alternatives (CEA)

Abstract

During glass production, phase separation can result in the formation of suspended liquid droplets, which can cause changes in the system rheology. In nuclear waste vitrification context, some new glassy matrices may present this phase separation matter, but the mechanisms controlling the viscosity changes have not yet been determined. Here, we measure the viscosity of a sodium-borosilicate melt containing dissolved MoO₃ at different temperatures and subject to different applied shear strain rates. We observe that (i) the viscosity increases sharply as the temperature decreases and (ii) at any constant temperature below 1000°C, the system presents non-Newtonian response. Using transmission electron microscope observations coupled with viscosity calculations, we interpret the cause of the observed changes as the result of phase separation. We show that the viscosity increase on cooling is in excess of the predicted temperature dependence for a homogeneous melt of the starting composition. The increase is due to the formation of a second phase and is controlled by chemical and structural modifications of the matrix during the loss of the elements that form the droplets. This work provides insights into the rheology of a system composed of two composition sets due to a miscibility gap.

KEYWORDS

conditioning, glass-forming melts, nuclear waste vitrification, process control, viscosity

1 | INTRODUCTION

The study of silicate melts is of primary importance in several natural and industrial processes. For example, silicates play a key role in volcanism.¹ Similarly, in industrial

settings, silicate melts are of paramount importance for glass production and for the vitrification of wastes.^{2,3} For the latter, the use of silicate melts containing high amounts of boron oxide (i.e., borosilicate glass) are the most common for vitrification of nuclear wastes.⁴ Not only in this

This is an open access article under the terms of the [Creative Commons Attribution-NonCommercial-NoDerivs](https://creativecommons.org/licenses/by-nc-nd/4.0/) License, which permits use and distribution in any medium, provided the original work is properly cited, the use is non-commercial and no modifications or adaptations are made.

© 2023 The Authors. *International Journal of Applied Glass Science* published by American Ceramics Society and Wiley Periodicals LLC.

industrial context, but also in natural contexts, borosilicates have been widely investigated and results for density, viscosity, interfacial tension, and water solubility are available.^{5–8} Vitrification is currently recognized as the standard treatment to immobilize nuclear high-level wastes (HLWs). To achieve this immobilization, the liquid waste is dried, calcined, and fed into a melter together with borosilicate glass frit.^{9,10} During high-temperature treatment, the viscosity of these systems plays a fundamental role in controlling several phenomena, such as melting, bath-to-glass conversion, particle aggregation, mass transfer, bubble removal, and the quality of the final product.^{11–19}

Glass-ceramic matrices are an alternative way to immobilize nuclear waste because higher amounts of HLWs can be vitrified and these matrices could offer a higher flexibility in the management of various waste streams. In such processes, different physicochemical transformations, such as bubble formation, liquid-liquid phase separation, and/or crystallization may take place.²⁰ The formation of secondary phases may induce modifications that critically affect the vitrification efficacy or the processing of the wastes.²⁰ First, secondary phases are typically non-stoichiometric, which means that their formation results in composition changes in the borosilicate matrix. Chemical modifications can result in structural changes that lead to either depolymerization or polymerization of the borosilicate network, which directly impacts the viscosity of the melt and the final multiphase material. Second, the physical presence of the secondary phase may also cause changes in viscosity via suspension effects.^{21–23} For instance, the presence of solid particles with immobile interfaces can induce shear-thinning behavior in silicates.²⁴ Similarly, droplets or bubbles with mobile interfaces can be deformed under flow, and shear-thinning rheological behavior can also be observed.^{21–23} At low rates of shear strain, bubbles or droplets may act like undeformed particles suspended in melts and cause a concomitant increase of the overall viscosity of the system.^{21–23} Whereas at high rates of shear strain the same bubbles or droplets may deform resulting in lower bulk viscosity when compared to the single liquid phase.^{21–23} This interplay between deformation and viscosity responses can be estimated via the capillary number.^{21–23}

In this work, we investigate which of the possible factors (physical suspension effects or chemical effects in the melt) dominates the viscosity changes of a particular glass melt of nuclear interest undergoing phase separation phenomena. We choose a sodium borosilicate glass melt containing MoO₃, which is a simplified and relevant composition for nuclear waste immobilization.²⁵ Molybdenum is a fission product coming from spent fuel reprocessing solutions, and has low solubility in borosilicate melts.²⁶ We chose a composition containing 1.5 mol% of molyb-

TABLE 1 Chemical composition of Mo-bearing borosilicate melts (in mol%)—Error is also displayed and represents the standard deviation of the mean on repeat measurements. The analyzed values by EPMA were subsequently converted to mol%.

Oxides	1.5 Mo-bearing glass (calculated values; mol%)	1.5 Mo-bearing glass (obtained via EPMA; mol%)
SiO ₂	62.54	62.4 ± 0.3
B ₂ O ₃	16.65	16.0 ± 0.2
Na ₂ O	19.31	20.1 ± 0.5
MoO ₃	1.50	1.5 ± 0.1

denum oxide (MoO₃) that starts to undergo liquid-liquid phase separation for temperatures below 1000°C.²⁵ We performed viscosity measurements followed by transmission electron microscope (TEM) analyses after quenching the material by casting on a cooled copper plate immediately followed by pressing from above with an upper second copper plate. In this work, using these experimental results coupled with a rheological approach, we aim to understand the main contributions for viscosity change upon liquid-liquid phase separation.

2 | MATERIAL AND METHODS

2.1 | Glass synthesis

The glasses were synthesized from a mixture of oxide reagents (SiO₂, MoO₃), together with borate (H₃BO₃), and carbonate (Na₂CO₃) precursor powders. These materials were homogenized at room temperature and 100 g of this mixture was melted at 1300°C under air in a Pt₈₀-Rh₂₀ crucible in a muffle furnace. The molten glass was then quenched by casting in a water-cooled copper hearth followed by a crushing on this hearth with a second copper plate. The theoretical chemical composition obtained by weighing the starting materials as well as the final glass composition analyzed via electron probe microanalyzer (EPMA) are displayed in Table 1.

2.2 | Electron microprobe

The chemical composition of the synthesized glass was measured with a CAMECA SX100 electron microprobe, using crystals LTAP for sodium and silicon, LPET for molybdenum, and LPC3 for boron. The electronic beam operating voltage was 12 kV, while the current was 10 nA. The analysis conditions were optimized in order to minimize sodium migration under the electron beam. The acquisition time was 70 s and the defocused beam size at 45 μm was chosen for the analysis. The final composition

is an average of 10 analyses. The chemical composition obtained using EPMA is displayed in Table 1.

2.3 | Viscosity measurements

Viscosity measurements were carried out at high temperature (~ 900 – 1125°C) under air with a concentric cylinder viscometer. The sample was melted into a $\text{Pt}_{80}\text{-Rh}_{20}$ crucible of ca. 27-mm inner diameter and ca. 54-mm height, which sits in a mullite cradle brick. A $\text{Pt}_{80}\text{-Rh}_{20}$ spindle of 9 mm in diameter, hanging from a rheometer head is submerged in the melt; the set-up is therefore a wide-gap system with 18-mm gap width. The viscometer head controls the rotation rate and measures the resulting torque. These measurements require ca. 21 cm^3 of glass melt. The temperature of the system is monitored using a type B thermocouple calibrated against a type S platinum-sheathed thermocouple submerged between measurements in the melt sample. Within the aforementioned temperature range, viscosity measurements were performed for 10 different temperatures (1125, 1099, 1074, 1046, 1020, 1000, 979, 958, 939, and 904°C). At each temperature, after thermal and mechanical stabilization of the system (ca. 40 min) the rheological behavior of the liquid was analyzed at increasing rotor speed from 0 to 100 rpm. The duration of each isothermal analysis is about 2 min and a total of 90 viscosity measurements points is acquired for each sample. The 2-min wait time was enough to obtain steady-state viscosity results^{21,25} The conversion from torque and rotation rate to shear stress and shear strain rate is done and the final viscosity at each point is obtained by dividing the shear stress σ by the shear strain rate $\dot{\gamma}$.

2.4 | TEM

High-resolution transmission electron microscopy analyses were performed with a JEOL JEM 2010F UPR22 microscope (CP2M Aix-Marseille University, France). The beam diameter is in the nanometer range under an accelerating voltage of 200 kV. The samples were crushed and dispersed in alcohol. They were then deposited on a copper grid. This equipment allows high resolution analyses to be performed (HRTEM).

3 | RESULTS AND DISCUSSION

3.1 | Rheological response

In Figure 1, we present the bulk viscosity of the Mo-bearing melts as a function of shear strain rate $\dot{\gamma}$ normalized by the maximum shear strain rate value $\dot{\gamma}_{\text{max}}$ (giving a normalised

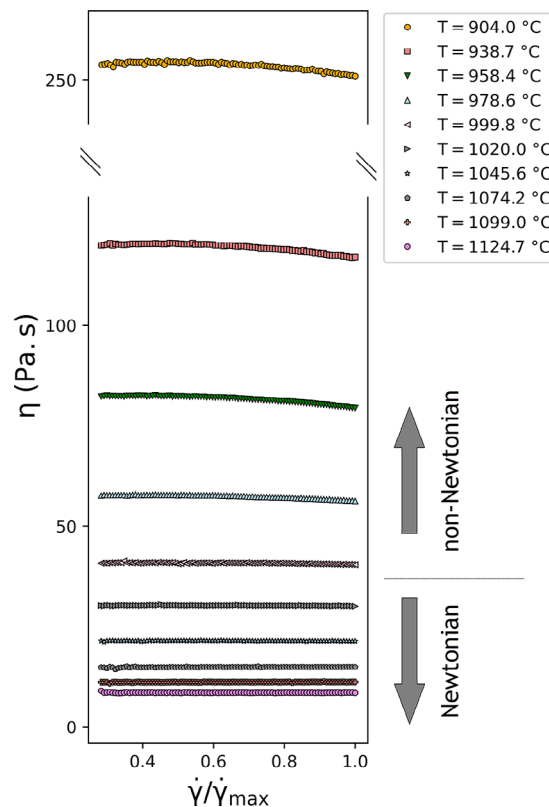


FIGURE 1 Viscosity η of a Mo-bearing melt at different temperatures as a function of shear strain rate normalized by its maximum value $\dot{\gamma}/\dot{\gamma}_{\text{max}}$.

rate $\dot{\gamma}/\dot{\gamma}_{\text{max}}$) for several temperatures. This normalization is simply for presentation purposes to align the rheological responses across all temperatures. In general, the viscosity of these silicate melts increases as temperature decreases and this behavior is discussed later (Sections 3.3 and 3.4). The figure displaying the non-normalized shear strain rate used in the experiments is presented in Figure S1. For experiments performed above 1000°C the viscosity does not depend on the shear rate, exhibiting a Newtonian behavior. By contrast, Mo-bearing samples analyzed at temperatures below 1000°C appear non-Newtonian with a viscosity that decreases as shear strain rate is increased, that is, shear-thinning^{21,22} While this shear-thinning effect is very small, it is clear that the amplitude of the viscosity decrease increases with decreasing temperature for temperature below 1000°C . Recently, using in situ scanning electron microscopy and viscosity measurements, Schuller et al.²⁵ estimated that for this same composition liquid-liquid phase separation occurs at temperatures below 1000°C . We therefore infer that the shear-thinning behavior may result from phase separation yielding secondary phase droplets, and that the amplitude of the shear thinning is likely to be a function of the volume fraction and size of suspended droplets of the secondary phase.²⁵ This interpretation is tested below.

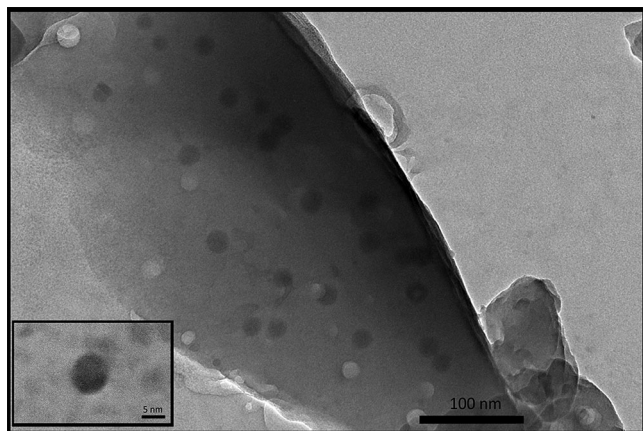


FIGURE 2 Transmission electron microscopic images of the quenched Mo-bearing borosilicate glass reveal a borosilicate matrix suspending Mo- and Na-rich droplets. The inset shows inter-plane fringes indicating crystalline character.

3.2 | Textural modifications

The quenched glass appears optically transparent and homogeneous to the naked eye, as observed elsewhere.²⁵ However, TEM analyses confirm that droplets of about 10 nm in diameter are present in a glassy borosilicate matrix (Figure 2). These nano-structures are spherical (aspect ratio of ~ 1) and unconnected throughout the silicate matrix, consistent with in situ homogeneous nucleation and growth.²⁷ The amplitude of the observed shear-thinning rheological response for system presenting droplets is small and it can be better understood through the capillary number which is given by $Ca = \eta_{\text{liquid}} a \dot{\gamma} / \sigma$, where η_{liquid} is the suspending liquid viscosity, a is the suspended droplet radius, $\dot{\gamma}$ is the shear strain rate, and σ is the surface tension. Under flow, viscous stresses $\tau_v \propto \eta_{\text{liquid}} \dot{\gamma}$ may cause mobile droplets to deform, while surface tension stresses $\tau_s \propto \sigma/a$ act to restore droplets to spherical. The capillary number can be understood as $Ca = \tau_v / \tau_s$ and therefore allows us to quantify the relative importance of those stresses. The current system has small droplet radius (cf. Figure 2; $a \approx 5$ nm). If we take the highest viscosity and shear strain rate measured as $\eta_{\text{liquid}} \approx 260$ Pa.s and $\dot{\gamma} \approx 100$ s⁻¹, respectively (Figure 1 and Figure S1), and a standard $\sigma \sim 0.004$ N/m for silicate melts and immiscible substances, then $Ca \lesssim 3.3 \times 10^{-2}$.^{23,28} At the lowest measured shear strain rates of $\dot{\gamma} \approx 10$ s⁻¹ and lowest values of melt viscosity of $\eta_{\text{liquid}} \approx 15$ Pa.s then $Ca \lesssim 1.9 \times 10^{-4}$. Even acknowledging that these calculations are approximate and that they do not account for the viscous forces' interior to the droplets, in all cases here, it is clear that the likely regime is $Ca \ll 1$. In this low capillary number regime, droplet deformation is difficult because surface tension stresses act to retain spherical droplets.

In the inset of Figure 2, the presence of interplane fringes indicates that some of the droplets underwent crystallization upon cooling.²⁹ This ease of crystallization after liquid-liquid phase separation has been already reported in the literature for synthetic silicate samples, due to modifications of nucleation parameters, such as the Gibbs free energy for nucleation and diffusivity of atoms in the separated phase.^{28,30} Several studies have focused on this family of glass compositions, and by coupling different experimental techniques, it has been observed that the droplets formed are composed of sodium molybdate.²⁹ X-ray diffraction reveals that the phase formed depends on the Mo content dissolved in the initial borosilicate melt. At low Mo amounts (less than 2 mol% MoO₃), Na₂MoO₄ is the dominant phase,^{25,29} while at high Mo amounts (greater than 2 mol% MoO₃), it gives way to the emergence of Na₂Mo₂O₇.²⁹ It is important to emphasize that crystallization takes place under cooling. At high temperatures, these droplets are found as liquid droplets due to the low melting point (relative to the experimental temperatures) of Na₂MoO₄ (687°C).^{20,31} Therefore, the crystalline phases observed in the final products represent the quenched evidence for phase separated liquid droplets that formed during the high-temperature experiments.

The amount of secondary phases (e.g., crystals, droplets, or bubbles) can be relatively easy to estimate on quenched glasses using microscopic techniques, such as optical microscopy, scanning electron microscopy, or transmission electron microscopy.^{18,32} However, at high temperatures (in situ), the amount of secondary phases in silicate melts is more challenging to estimate. Some studies have used impedance spectroscopic methods at high temperature to infer the fractions of bubbles and crystals that form.^{33,34} However, this in situ estimation has never been achieved for the system under scrutiny here. For a similar system (containing 2 mol% MoO₃) and using X-ray diffraction coupled with Rietveld refinement, Nicoleau et al.²⁹ estimated that the droplet volume was 0.9 vol.%. Here, considering a stoichiometric mass balance which we get from the initial borosilicate melt composition ($\rho_{\text{borosilicate}} \sim 2.25$ g.cm⁻³)¹⁹ and a fixed fraction of Na₂MoO₄ ($\rho_{\text{Na}_2\text{MoO}_4} = 3.78$ g.cm⁻³) until the remaining molybdenum is small enough to cease liquid-liquid phase separation, we obtain 3.21 vol.% as the maximum volume fraction of droplets.

3.3 | Effect of phase separation on viscosity

Several glassy materials may undergo phase separation in industrial or natural contexts; phase separation consists of the formation of two sets of compositions on the same

liquid phase, that is, two local minima on the Gibbs energy curve. This phenomenon is non-stoichiometric by definition. When the second phase is formed, the rheological behavior of the system is affected by two main factors: (i) the physical presence of the secondary phase changes the rheology of the mixture via suspension effects and (ii) the chemical modifications that the matrix undergoes during the phase separation process can result in a rheological change in the primary groundmass liquid.^{21,22} In this section, we evaluate which of these factors has the dominant impact on the viscosity increase observed in our MoO₃-bearing borosilicate melt.

To characterise the single-liquid viscosity, η_{liquid} , we apply both the Vogel–Fulcher–Tammann (VFT)^{35–37} or the Mauro–Yue–Ellison–Gupta–Allan (MYEGA)³⁸ approach. These models are respectively:

$$\log_{10}(\eta_{\text{liquid}}) = A_{\text{VFT}} + \frac{B_{\text{VFT}}}{T - C_{\text{VFT}}}, \quad (1)$$

$$\log_{10}(\eta_{\text{liquid}}) = A_{\text{MYEGA}} + \frac{B_{\text{MYEGA}}}{T} \exp\left(\frac{C_{\text{MYEGA}}}{T}\right). \quad (2)$$

In both models, there are three fit parameters, A, B, and C (where we use a subscript to differentiate these between the two models; see Equations 1 and 2). In both cases, the A parameter (A_{VFT} and A_{MYEGA} , respectively) represent the logarithm of the viscosity at infinite temperature, and the B parameter (B_{VFT} and B_{MYEGA} , respectively) are related to the concept of an activation energy—here, the activation energy for viscous flow. A key difference between these two models is the physical interpretation of the C parameter (C_{VFT} and C_{MYEGA} , respectively). In the VFT model, the C parameter represents the low-temperature limit where the viscosity diverges to infinity. In the MYEGA model, the C parameter represents the degrees of freedom per atom with rising temperature.

In order to reduce the number of variables that must be minimized in order to use Equation (1) or Equation (2), we apply the concept of a universal A_{VFT} and A_{MYEGA} that would be the same value regardless of the glass composition.³⁹ Russell et al.,³⁹ propose universal values $A_{\text{VFT}} = -4.80$ and $A_{\text{MYEGA}} = -3.25$ (both in units of $\log_{10}(\text{Pa}\cdot\text{s})$). Using this constraint, we fit both Equations (1) and (2) to the experimental data collected here. The fits were constrained by considering the experimental values for which we have independent evidence (e.g., Figure 1) that there was just one liquid phase involved. Here, this means that the fits are restricted to experimental data collected above 1000°C. For this purpose, the viscosity values obtained below the phase separation temperature onset were eliminated and we use only temperatures 1020.0, 1045.6, 1074.2, 1099.0, 1124.7°C. The

TABLE 2 Fitting parameters for VFT and MYEGA equations for the viscosity data without suspended second phase.

Viscosity equation	A ^a	B	C
Units	log ₁₀ (Pa.s)	K	K
VFT (Equation 1)	−4.80	6783.07 ± 78.86	212.49 ± 13.13
MYEGA (Equation 2)	−3.25	3271.94 ± 41.13	808.57 ± 16.86

^aImposed values using Russell et al.³⁹

results of these fit procedures are given in Table 2 in which the relative uncertainties relate to the confidence on the fit result.

In Figure 3, we show the experimental viscosity data as a function of temperature. The experimental data correspond to the limiting viscosity at low and high shear strain rates (see Figure 1). Clearly, above 1000°C, not only do both of these limiting viscosity values coincide, but the models (Equations 1 and 2) match well. The data collected at temperatures below 1000°C are systematically higher than the extrapolation of the best-fit viscosity models. We note that within the errors of the fits, both equations yield the same result. Deviations of the experimental values from the fitting curves grow with decreasing temperature. We attempted to refine the fitting by measuring the viscosity of the single Mo-bearing supercooled liquid around the glass transition temperature. However, our sample might have undergone phase separation during this procedure and therefore the above-mentioned fitting operation is the best that we could perform so far. Therefore, we must recognize here that this extrapolation of the fit performed using VFT and MYEGA equations may contain associated errors.

Suspended phases that have mobile interfaces (e.g., bubbles or droplets) may be deformed under shear and consequently change the viscosity of the suspensions. The net effect may be such that the viscosity is higher than the single liquid viscosity at low rates of shear strain where the suspended phase is not significantly deformed. However, at higher relative rates of shear strain, the suspension viscosity can be lower than the liquid alone.²³ Our data suggest that the viscosity of the samples deformed at <1000°C were unlikely to be lower than the liquid viscosity such that $\dot{\gamma}_{\text{max}}$ appears to be sufficiently low that the suspended phase always increased the viscosity of the suspension. At the lowest measured temperature (~900°C), we observe some shear thinning, implying that $\dot{\gamma}_{\text{max}}$ may be sufficient to see the onset of droplet deformation during our experiments. We observe that the difference between low and high shear viscosity values gets larger as the temperature decreases, since liquid droplets unmix at low-temperature conditions.²⁵

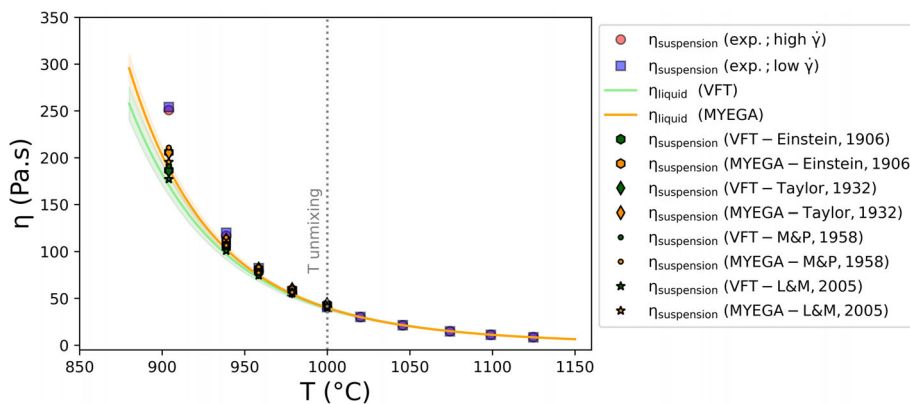


FIGURE 3 Viscosity of MoO_3 -bearing melts displaying phase separation below $\sim 1000^\circ\text{C}$. The colored lines represent the single liquid viscosity η_{liquid} estimated using the VFT and MYEGA equations. The squared and circled symbols represent the experimental values obtained for the system containing droplets of sodium molybdate at low and high shear strain regimes respectively. The suspension viscosity $\eta_{\text{suspension}}$ using different models were estimated considering the maximum droplet fraction obtained via stoichiometric calculation and suspension effects on viscosity.

In the regime where volume fraction of suspended particles is small and the particles^{21–23,40–43} are not deformed (see the capillary number analysis presented earlier, which argues that the droplets here are in the $\text{Ca} \ll 1$ regime), some models for suspension/emulsion viscosity can be applied

$$\eta_{\text{suspension}} = \eta_{\text{liquid}}(1 + 2.5\phi_{\text{droplet}}),$$

$$\eta_{\text{suspension}} = \eta_{\text{liquid}}\left(1 + 2.5 \left(\frac{k + 0.4}{k + 1}\right) \phi_{\text{droplet}}\right),$$

$$\eta_{\text{suspension}} = \eta_{\text{liquid}} \left(1 - \frac{\phi_{\text{droplet}}}{\phi_{\text{max}}}\right)^{-2}, \text{ and}$$

$$\eta_{\text{suspension}} = \eta_{\text{liquid}} (1 - \phi_{\text{droplet}})^{-1};$$

in which ϕ_{droplet} , ϕ_{max} , and k represent the droplet volume fraction, the maximum packing fraction for spherical particles ($\phi_{\text{max}} = 0.585$) in which the suspension becomes ‘jammed’, and the ratio between the suspending liquid viscosity and the viscosity of the droplet liquid ($k \gg 1$).^{21–23, 41, 42} In Figure 3, we show the values of droplet-bearing melt viscosity considering only this physical effect of the secondary phase according to the just mentioned equation. These results are displayed as green (for VFT) and orange (for MYEGA) using different symbols in Figure 3. Here, we considered the worst-case scenario for viscosity increase due to the physical presence of the secondary phase, in which the system consumed all available MoO_3 and formed the maximum possible fraction of droplets ($\phi_{\text{droplet}} = 3.21$ vol.%), as previously discussed. This analysis has been done for both VFT and MYEGA liquid viscosities. The initial idea was to use current viscosity models to estimate the viscosity evolution while the system undergoes phase separation. The well-known

viscosity models are not applicable for this present composition, since they do not consider MoO_3 as an individual input oxide or consider it in the input called ‘others’ (for which ‘others’ refers to the sum of the minor oxides in the molten glass). We checked viscosity models for silicate melts, for example, Hui et al.,⁴⁴ Giordano et al.,⁴⁵ and Ferkl et al.,⁴⁶ but none of them considers MoO_3 as an independent input oxide. Recently, Cassar⁶⁰ published a multitask neural network that predicts well the evolution of the studied molten glass composition, but it does overestimate the single liquid borosilicate viscosity (further analyses in section 3.5).

It can also be observed from Figure 3 that the difference between the low and high viscosity experimental values is significantly lower than the difference between the average of the calculated suspension values and the expected value for the viscosity in the case for which no phase separation occurs (estimated via the VFT and MYEGA equations). By observing the sole physical contribution to the viscosity increase, green and orange symbols in Figure 3, it can be stated the physical presence of droplets has minor effect on controlling the viscosity augmentation observed during phase separation. Figure 4 illustrates these aforementioned comparisons. It displays that these differences between low- and high-shear strain rate zones as well as the difference between the average of the measured viscosity values and the estimated values from the VFT and MYEGA model fits. We also plot the values representing the difference between the viscosity of the suspension for which only the physical contribution of the droplets is accounted for and the estimated liquid viscosity for the case of no phase separation, for both the VFT and MYEGA models. Figure 4 confirms the idea that just the physical presence of suspended droplets does not explain the observed viscosity increase upon phase separation. Thus,

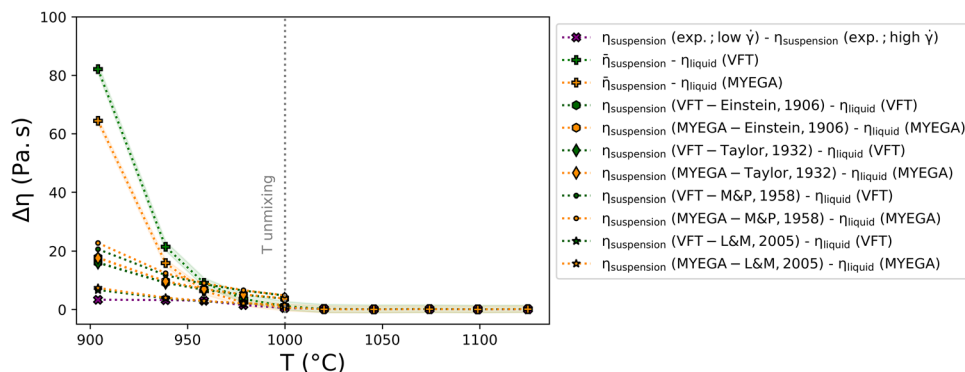


FIGURE 4 Difference between experimental and calculated viscosity values showing that the viscosity change due to the physical presence of the suspended droplets is less relevant than the viscosity increase due to chemical modification of the remaining matrix.

the structural changes caused by the extraction of sodium and molybdenum to form sodium molybdate droplets must have greater impact than the physical presence of dispersed nano-sized droplets.

3.4 | Structural changes caused by the liquid-liquid phase separation in a MoO₃-bearing melt

We have observed that our calculated bound for the physical contribution of suspended nano-droplets does not explain the increase in viscosity observed experimentally, and that chemical changes in the remaining silicate matrix must be controlling the observed viscosity increase. In this section, we present evidence that under the current secondary phase formation (Na₂MoO₄), the remaining borosilicate liquid will be more polymerized, and this justifies the observed viscosity increase.

Several studies have been devoted to the understanding of the role of molybdenum and sodium in the glass network.^{47–52} Molybdenum may have different oxidation states in glasses, but the most thermodynamically stable found in oxide glasses synthesized under air conditions is in the form of Mo⁶⁺.^{53,54} Molybdenum environment in silicate and borosilicate glasses have been investigated recently using different spectroscopic techniques.^{29,49–52,55} Molybdenum is tetrahedrally coordinated to oxygen as [MoO₄]²⁻ units distributed in depolymerized zones of the glass rich in charge-compensating cations (e.g., Na⁺).^{26,27,29,50} These molybdate groups avoid connection with the borosilicate network.⁴⁹ This particular structural environment of molybdenum with no direct connection with the borosilicate network favors liquid-liquid phase separation phenomenon to take place.

Martineau et al.⁵² employed ²⁹Si-¹¹B nuclear magnetic resonance (NMR) Rotational Echo Double Resonance spectroscopy, to argue that the borosilicate network sepa-

rates at the atomic scale in the presence of molybdenum oxide, that is, atomic local segregation. They showed a decrease of the B-Si(Q⁴) connections with an increase of the Mo content and thus the weaker presence of mixing zones. Nicoleau et al.²⁹ investigated the local structure of similar glasses using magic angle spinning ²⁹Si and ¹¹B NMR spectroscopy techniques. Their study confirms the impact of the addition of molybdenum oxide on the polymerization of the silicate network, since during its addition alkali segregation around the Mo units is observed and that [MoO₄]²⁻ units mobilize two sodium atoms to compensate their charge leading initially to a decrease of non-bridging oxygens (NBO) (even for very low MoO₃ contents, that is, 0.5 mol%) as well as BO₄⁻ species when the amount of separated phases increases (MoO₃ content = 2 mol%). A further consequence of this polymerization is reflected in the chemical durability of the glasses in the initial corrosion rate regime. It has been observed in their study an increase of the glass durability with increasing molybdenum content, that can be interpreted as resulting from the decrease of NBOs and thus polymerization of the remaining glassy network. Glass durability increases with MoO₃ content, which is consistent with a increase in the network polymerization of the remaining glassy matrix arising from a concomitant decrease in NBO. Therefore, this family of glass appear to possess a heterogeneous structure at the nanometer scale, with [MoO₄]²⁻ entities together with alkali cation regions and other regions with silica tetrahedra-based polymerized domains.^{49–51}

The heterogeneities in nanoscale, which are not yet phases with sharp interface such as nano-droplets or nanocrystals, have been already observed in other silicate systems^{56–58}; however, their effect on viscosity is still unknown. For the studied case, these nano-heterogeneities cause local polymerized and depolymerized regions. While regions near Mo atoms get depolymerized by the alkalis, the regions far away get polymerized by the absence of these atoms. Therefore, in a situation prior to the phase

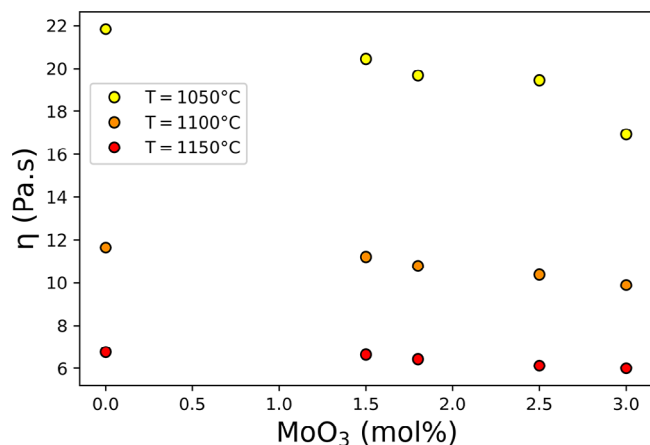


FIGURE 5 Viscosity of different borosilicate melts as a function of MoO₃ oxide for three temperatures in which liquid-liquid phase separation is not present. Data show the dependence of viscosity on MoO₃ amount. They were obtained from Schuller et al.²⁵

separation event, nothing can be stated regarding the viscosity change as a function of these nano-heterogeneities since a sharp interface between these zones does not exist yet. However, the formation of a secondary liquid composition with a well-defined interface and composed by sodium and molybdenum will certainly cause polymerization of the remaining glass matrix, and therefore viscosity increase.

In order to illustrate the effect of molybdenum on the viscosity of this family of glass melt, we collated data from Schuller et al.²⁵ for molten borosilicate glasses with varying MoO₃ mol% (Figure 5). These data were obtained in the regions of temperature in which no phase separation happens (i.e., no shear-thinning behavior was detected).²⁵ Moreover, it is important to emphasize that all of these compositions have excess of alkali and therefore all charges are compensated. An increase of molybdenum content dissolved in the melt causes a decrease of viscosity, as would be expected by the polymerization behavior discussed in this section. The effect of molybdenum on the melt viscosity is more pronounced for relatively low-temperature regions. This behavior, which is similar to iron effects in magmatic liquids, is linked to the chemical and structural effects that influences the configurational entropy and therefore viscosity.^{59–61}

The effect of sodium on melt structure and viscosity of silicate and borosilicate melts is well studied. Sodium can have two roles in silicate and borosilicate networks. In the presence of entities that require charge compensation (e.g., Al³⁺ ions), sodium generally has a charge compensator function. On the other hand, in scenarios in which charges are already compensated or there is no need for compensation, sodium ions have a network modifier role

in silicate melts, promoting formation of NBO.⁴⁸ Neuville⁶² and Le Losq et al.⁶³ presented data that show the influence of sodium on structure and viscosity of a family of soda-silicate melts for varying sodium content. For glass systems that do not require charge compensation or glasses with excess alkali, the addition of Na₂O leads to the breaking of Si – O – Si bonds and formation of NBO, inducing therefore a decrease in viscosity.⁴⁸ Although there are boron and molybdenum in the studied system, this current studied system is an excess of alkali and therefore, sodium extraction for the borosilicate matrix during droplet formation will cause strengthen of the network and increase of viscosity.

3.5 | Viscosity increase of sodium-molybdenum borosilicate undergoing phase separation phenomenon

So far we have showed that the studied sodium-molybdenum borosilicate melt (cf. Table 1) shows liquid-liquid phase separation below 1000°C and at these temperatures, the observed viscosity increase was higher than the expected by the extrapolation of the VFT and MYEGA viscosity laws. We discussed the structural effects linked to the formation of droplets of Na₂MoO₄, and consequently extraction of MoO₃ and Na₂O from the borosilicate matrix. Here, our goal is to present numerical and experimental evidence that borosilicate samples depleted on molybdenum and sodium do present an increase in viscosity proportional to the one observed in the current studied system.

Cassar⁴⁰ recently published multitask deep neural network model called “GlassNet” that predicts several glass properties, including viscosity of molten glasses. This model is suitable for the study of our system since it has been trained with enough compositions containing SiO₂, B₂O₃, Na₂O, and MoO₃ as independent input parameters. Figure 6 displays the results of a simulation using this mentioned model to show the shift in viscosity between (i) the initial borosilicate melt composition (herein called ‘original’), (ii) the original composition depleted on 1.5 mol% of molybdenum oxide, (iii) the original composition depleted on 1.5 mol% of sodium oxide, and (iv) the original composition depleted on both Na₂O and MoO₃ (herein called ‘depleted’). Here, our goal is to present the general trend that occurs in the borosilicate matrix viscosity upon phase separation of the studied type, in which Na₂O and MoO₃ are extracted from the borosilicate composition upon droplet formation. As expected according to the discussion part of the previous section, an extraction of these two elements does cause a viscosity increase of this family of glass. It is interesting to observe that for this studied

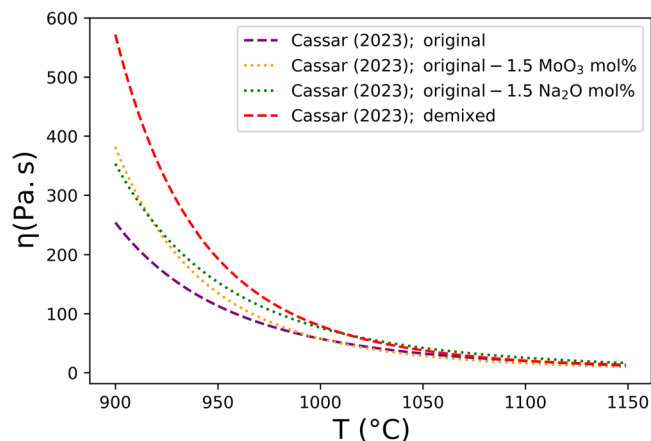


FIGURE 6 Viscosity as a function of temperature for the initial homogeneous molten borosilicate and for the homogeneous matrix considering the stoichiometric extraction of sodium, molybdenum, and the stoichiometric depletion of both together according to the droplet composition and amount given here in this work. Viscosity values were obtained using GlassNet neural network published in Cassar.⁴⁰

TABLE 3 Chemical composition of borosilicate melts (in mol%): the first column refers to the matrix composition after subtraction of Na_2O and MoO_3 (see text for stoichiometry), and second column is the Mo-free glass obtained from Schuller et al.²⁵

Oxides	Matrix of demixed glass (calculated values; mol%)	Mo-free glass (Schuller et al. 2023; mol%)
SiO_2	64.47	63.49
B_2O_3	17.16	16.91
Na_2O	18.36	19.60
MoO_3	0.00	0.00

temperature range and amount of droplets, the extraction of these two oxides separated have a similar effect on viscosity augmentation.

Experimentally, Schuller et al.²⁵ recently published a data set of viscosity of the same family of glass containing SiO_2 , B_2O_3 , Na_2O , and MoO_3 . They progressively added molybdenum to these materials and the viscosity of these melts are available therein. We used their data of the Mo-free borosilicate in order to compare with experimental data of this cur study that presents phase separation phenomenon. Our goal is to verify if a homogenous melt with very similar composition to the final matrix composition of the samples that presented phase separation has similar viscosities. This composition from Schuller et al.²⁵ is very similar to the composition of the homogeneous borosilicate matrix after the extraction of sodium and molybdenum to form the droplets and both of them are displayed in Table 3. Figure 7 shows the viscosity as a function of temperature for these two compositions. A

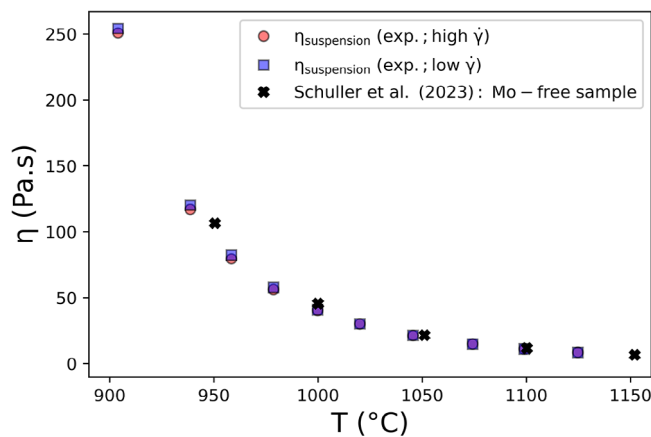


FIGURE 7 Viscosity as a function of temperature for the borosilicate composition that undergoes phase separation and contains molybdenum and sodium along with the viscosity data from Schuller et al.²⁵ for a homogeneous molten Mo-free borosilicate with similar composition to the borosilicate matrix after phase separation phenomenon.

excellent agreement for these two similar compositions has been found, and therefore it also supports our idea that the chemical composition of the primary groundmass liquid is the main reason controlling the viscosity of this family of melts that undergo liquid-liquid phase separation extracting molybdenum and sodium.

4 | CONCLUSION

We studied the rheological response of Mo-bearing borosilicate melt undergoing phase separation phenomenon for varying temperatures and shear strain rates. We observed that for the temperature range in which phase separation takes place, there is an increase of viscosity higher than that estimated by the extrapolation of viscosity models as well as superior to the estimation via suspension effects considering mobile droplets. By combining TEM observations with calculations on viscosity of silicate melts containing mobile particles, we inferred the main factors controlling the observed viscosity increase. The observed viscosity augmentation for the samples containing nano-droplets of Na_2MoO_4 cannot be solely justified by their physical presence. We discuss these results in light of the structure of this family of molybdenum-bearing glasses and propose that the observed viscosity increase is controlled by chemical modification of the remaining borosilicate matrix. Following this logic, in an industrial scenario that would present suspended droplets, even if they form at low volume fractions—too low for a bulk suspension increase in viscosity—, the associated modification of the melt composition may lead to a substantial viscosity increase. Such phenomena, involving different chemistry,

may equally well occur in other molten glasses as well as in natural volcanic systems during eruption.

ACKNOWLEDGMENTS

LP is grateful for the support of the Alexander von Humboldt Foundation. Sophie Schuller thanks CEA, ORANO, and EDF for their financial support. The authors acknowledge the support of the European Research Council (ERC) 2018 ADV, grant number: 834225 (EAVESDROP) and the São Paulo Research Foundation (FAPESP), grant number: 2021/03374–5 (RFL). The authors thank Martiane Cabié (CP2M, Aix-Marseille University) for HRTEM analyses, Janine Birnbaum for discussions on rheology, and Emmanuelle Brackx (CEA, DES, ISEC, Montpellier University, Marcoule, France) for EPMA analyses.

Open access funding enabled and organized by Projekt DEAL.


ORCID

Luiz Pereira  <https://orcid.org/0000-0001-9555-0352>


Sophie Schuller  <https://orcid.org/0000-0002-4511-4568>

Fabian B. Wadsworth  <https://orcid.org/0000-0002-5341-208X>

Jérémy Vasseur  <https://orcid.org/0000-0002-0783-5065>

Ricardo F. Lancelotti  <https://orcid.org/0000-0002-6111-6520>

Stéphane Gossé  <https://orcid.org/0000-0002-1213-6752>

Donald B. Dingwell  <https://orcid.org/0000-0002-3332-789X>

REFERENCES

- Dingwell DB. Volcanic dilemma—flow or blow? *Science*. 1996;273(5278):1054–55.
- Cable M. A century of developments in glassmelting research. *J Am Ceram Soc*. 1998;81(5):1083–94.
- Donald I. Glass and ceramic based. systems and general processing methods. Waste immobilization in glass and ceramic based hosts: radioactive, toxic and hazardous wastes. Chippenham, Wiltshire, U.K: John Wiley & Sons Ltd.; 2010. p. 57–71.
- Plodinec J. Borosilicate glasses for nuclear waste immobilization. *Glass Technol*. 2000;41:186–92.
- Knoche R, Dingwell DB, Webb SL. Melt densities for leucogranites and granitic pegmatites: partial molar volumes for SiO₂, Al₂O₃, Na₂O, K₂O, Li₂O, Rb₂O, Cs₂O, MgO, CaO, SrO, BaO, B₂O₃, P₂O₅, F₂O–1, TiO₂, Nb₂O₅, Ta₂O₅, and WO₃. *Geochim Cosmochim Acta*. 1995;59(22):4645–52.
- Dingwell D, Knoche R, Webb S, Pichavant M. The effect of B₂O₃ on the viscosity of haplogranitic liquids. *Am Mineral*. 1992;77:457–61.
- Veksler IV, Kähn J, Franz G, Dingwell DB. Interfacial tension between immiscible liquids in the system K₂O–FeO–Fe₂O₃–Al₂O₃–SiO₂ and implications for the kinetics of silicate melt unmixing. *Am Mineral*. 2010;95(11–12):1679–85.
- Holtz F, Dingwell DB, Behrens H. Effects of F, B₂O₃ and P₂O₅ on the solubility of water in haplogranite melts compared to natural silicate melts. *Contrib Mineral Petrol*. 1993;113(4):492–501.
- Pinet O, Vernaz E, Ladirat C, Gin S. Nuclear waste vitrification. *Encyclopedia of glass science, technology, history, and culture*. Hoboken, New Jersey: John Wiley & Sons Ltd.; 2021. p. 1205–18.
- Gin S, Jollivet P, Tribet M, Peugeot S, Schuller S. Radionuclides containment in nuclear glasses: an overview. *Radiochim Acta*. 2017;105.
- Lee S, Cutforth DA, Mar D, Klouzek J, Ferkl P, Dixon DR, et al. Melting rate correlation with batch properties and melter operating conditions during conversion of nuclear waste melter feeds to glasses. *Int J Appl Glass Sci*. 2021;12(3):398–414.
- Hrma P, Pokorny R, Lee S, Kruger AA. Heat transfer from glass melt to cold cap: melting rate correlation equation. *Int J Appl Glass Sci*. 2019;10(2):143–50.
- Pokorny R, Hrma P. Model for the conversion of nuclear waste melter feed to glass. *J Nucl Mater*. 2014;445(1):190–99.
- Pereira L, Vasseur J, Wadsworth FB, Trixler F, Dingwell DB. Interparticle and Brownian forces controlling particle aggregation and rheology of silicate melts containing platinum-group element particles. *Sci Rep*. 2022;12(1):9226.
- Machado N, Pereira L, Neyret M, Lemaitre C, Marchal P. Influence of platinum group metal particle aggregation on the rheological behavior of a glass melt. *J Nucl Mater*. 2022;563:153618.
- Pigeonneau F, Pereira L, Laplace A. Mass transfer around a rising bubble in a glass-forming liquid involving oxidation-reduction reaction: numerical computation of the Sherwood number. *Chem Eng Sci*. 2021;232:116382.
- Pigeonneau F, Pereira L, Laplace A. Dynamics of rising bubble population undergoing mass transfer and coalescence in highly viscous liquid. *Chem Eng J*. 2023;455:140920.
- Pereira L, Podda O, Fayard B, Laplace A, Pigeonneau F. Experimental study of bubble formation in a glass-forming liquid doped with cerium oxide. *J Am Ceram Soc*. 2020;103(4):2453–62.
- Pereira L, Klouzek J, Vernerová M, Laplace A, Pigeonneau F. Experimental and numerical investigations of an oxygen single-bubble shrinkage in a borosilicate glass-forming liquid doped with cerium oxide. *J Am Ceram Soc*. 2020;103(12):6736–45.
- McCloy J, Schuller S. Vitrification of wastes: from unwanted to controlled crystallization, a review. *Comptes Rendus Géosciences*. 2022;354:121–60.
- Mader H, Llewellyn E, Mueller S. The rheology of two-phase magmas: a review and analysis. *J Volcanol Geotherm Res*. 2013;257:135–58.
- Kolzenburg S, Chevrel MO, Dingwell DB. Magma/suspension rheology. In: Neuville DR, Henerson GS, Dingwell DB, editors. *Reviews in mineralogy and geochemistry: geological melts*. Chantilly, Virginia, U.S.A: Mineralogical Society of America Geochemical Society; 2022.
- Truby JM, Mueller SP, Llewellyn EW, Mader HM. The rheology of three-phase suspensions at low bubble capillary number. *Proc Math Phys Eng Sci*. 2015;471:20140557–81.
- Vasseur J, Wadsworth F, Dingwell DB. Shear thinning and brittle failure in crystal-bearing magmas arises from local non-Newtonian effects in the melt. *Earth Planet Sci Lett*. 2023;603:117988–97.
- Schuller S, Benigni P, Gossé S, Bégaud-Bordier S, Mikaelian G, Podor R, et al. Liquid-liquid phase separation in borosilicate glass enriched in MoO₃ – experimental investigations and thermodynamic calculations. *J Non-Cryst Solids*. 2023;600:121997.

26. Schuller S, Pinet O, Penelon B. Liquid–liquid phase separation process in borosilicate liquids enriched in molybdenum and phosphorus oxides. *J Am Ceram Soc.* 2011;94(2):447–54.
27. Schuller S. Phase separation processes in glass. In: Neuville D, Cormier L, Caurant D, Montagne L, editors. *From glass to crystal: nucleation, growth and phase separation: from research to applications.* Les Ulis, Ile de France, France: EDP Sciences; 2017. p. 125–54.
28. Zanutto E. Effect of liquid phase separation on crystal nucleation in glass-formers. Case closed. *Ceram Int.* 2020;46(16):24779–91.
29. Nicoleau E, Schuller S, Angeli F, Charpentier T, Jollivet P, Le Gac A, et al. Phase separation and crystallization effects on the structure and durability of molybdenum borosilicate glass. *J Non-Cryst Solids.* 2015;427:120–33.
30. Höche T, Mäder M, Bhattacharyya S, Henderson G, Gemming T, Wurth R, et al. ZrTiO₄ Crystallization in Nanosized Liquid-Liquid Phase Separation Droplets in a Glass- A Quantitative XANES Study. *CrystEngComm.* 2011;13:2550–56.
31. Uruga K, Tsukada T, Usami T. Generation mechanism and prevention method of secondary molybdate phase during vitrification of PUREX wastes in liquid-fed ceramic melter. *J Nucl Sci Technol.* 2020;57(4):433–43.
32. Zanutto E. Surface nucleation in a diopside glass. *J Non-Cryst Solids.* 1991;130(2):217–19.
33. Pereira L, Neyret M, Laplace A, Pigeonneau F, Nuernberg R. Inferring bubble volume fraction in a glass melt through in situ impedance spectroscopy measurements. *Int J Appl Glass Sci.* 2021;12(3):358–66.
34. Nuernberg R, Bello T, Fokin V, Zanutto E, Rodrigues ACM. Non-stoichiometric crystallization of Li₂SiO₃-CaSiO₃ glasses: residual glass composition from ionic conductivity. *J Non-Cryst Solids.* 2019;510:158–65.
35. Vogel H. Das temperaturabhängigkeitsgesetz der viskosität von flüssigkeiten. *Phys Z.* 1921;22:645.
36. Fulcher GS. Analysis of recent measurements of the viscosity of glasses. *J Am Ceram Soc.* 1925;8(6):339–55.
37. Tammann G, Hesse W. Die abhängigkeit der viskosität von der temperatur bei unterkühlten flüssigkeiten. *Z Anorg Allg Chem.* 1926;156(1):245–57.
38. Mauro JC, Yue Y, Ellison AJ, Gupta PK, Allan DC. Viscosity of glass-forming liquids. *Proc Natl Acad Sci.* 2009;106(47):19780–84.
39. Russell JK, Hess K-U, Dingwell DB. Chapter 18: Models for viscosity of geological melts. In: Daniel RN, Grant SH, Donald BD, editors. *Geological Melts.* p. 872022.
40. Cassar DR. GlassNet: a multitask deep neural network for predicting many glass properties. *Ceram Int.* 2023;49:36013–24.
41. Llewellyn EW and Manga M. Bubble Suspension Rheology and Implications for Conduit Flow. *J. Volcanol. Geotherm. Res.,* 2005;143:205–17.
42. Farah MA, Oliveira RC, Caldas JN, Rajagopal K, Viscosity of water-in-oil emulsions: Variation with temperature and water volume fraction. *J. Pet. Sci. Eng.,* 2005;48(3):169–84.
43. Birnbaum J, Lev E, Llewellyn EW, Rheology of three-phase suspensions determined via dam-break experiments. *Proceedings of the Royal Society A: Mathematical, Physical and Engineering Sciences,* 2021;477(2254):20210394.
44. Hui H, Zhang Y. Toward a general viscosity equation for natural anhydrous and hydrous silicate melts. *Geochim Cosmochim Acta.* 2007;71(2):403–16.
45. Giordano D, Russell JK, Dingwell DB. Viscosity of magmatic liquids: a model. *Earth Planet Sci Lett.* 2008;271(1):123–34.
46. Ferkl P, Hrma P, Kruger A. Parsimonious viscosity–composition relationships for high-temperature multicomponent glass melts. *J Asian Ceram Soc.* 2022;10(1):83–98.
47. Henderson GS, Stebbins JF. The short-range order (SRO) and structure. In: Neuville Daniel R, Henderson GS., Dingwell DB, editors. *Chantilly, Virginia, U.S.A: Geological Melts.* 2022.
48. Neuville DR, Le Losq C. Link between medium and long-range order and macroscopic properties of silicate glasses and melts. In: Neuville DR, Henderson, GS, Dingwell DB, editors. *Geological Melts;* 2022.
49. Calas G, Le Grand M, Galois L, Ghaleb D. Structural role of molybdenum in nuclear glasses: an EXAFS study. *J Nucl Mater.* 2003;322(1):15–20.
50. Farges F, Siewert R, Brown GE Jr., Guesdon A, Morin G. Structural environments around molybdenum in silicate glasses and melts. I. influence of composition and oxygen fugacity on the local structure of molybdenum. *Can Mineral.* 2006;44(3):731–53.
51. Caurant D, Majérus O, Fadel E, Quintas A, Gervais C, Charpentier T, et al. Structural investigations of borosilicate glasses containing MoO₃ by MAS NMR and Raman spectroscopies. *J Nucl Mater.* 2010;396(1):94–101.
52. Martineau C, Michaelis VK, Schuller S, Kroecker S. Liquid–liquid phase separation in model nuclear waste glasses: a solid-state double-resonance NMR study. *Chem Mater.* 2010;22(17):4896–903.
53. Short RJ, Hand RJ, Hyatt NC. An investigation into the oxidation state of molybdenum in simplified high level nuclear waste glass compositions. *MRS Online Proc Libr.* 2003;807:169.
54. Pereira LFP, Bodiang K, Nunes EHM, Mear FO, Delevoye L, Montagne L. Molybdenum influence on the mixed-alkali effect of lithium–sodium phosphate glasses. *J Phys Chem C.* 2018;122(28):15886–91.
55. Short RJ, Hand RJ, Hyatt NC, Möbus G. Environment and oxidation state of molybdenum in simulated high level nuclear waste glass compositions. *J Nucl Mater.* 2005;340(2):179–86.
56. Cormier L. From nanoscale heterogeneities to nanolites: cation clustering in glasses. *CR Phys.* 2023;24:1–15.
57. Dargaud O, Cormier L, Menguy N, Patriarche G. Multi-scale structuration of glasses: observations of phase separation and nanoscale heterogeneities in glasses by Z-contrast scanning electron transmission microscopy. *J Non-Cryst Solids.* 2012;358(10):1257–62.
58. Dargaud O, Cormier L, Menguy N, Patriarche G, Calas G. Mesoscopic scale description of nucleation processes in glasses. *Appl Phys Lett.* 2011;99(2):021904.
59. Neuville DR, Richet P. Viscosity and mixing in molten (Ca, Mg) pyroxenes and garnets. *Geochim Cosmochim Acta.* 1991;55(4):1011–19.
60. Richet P, Neuville DR. Thermodynamics of silicate melts: configurational properties. In: Saxena SK, editor. *Thermodynamic data: systematics and estimation.* New York, NY: Springer New York; 1992. p. 132–61.
61. Le Losq C, Cicconi MR, Neuville DR. Iron in silicate glasses and melts. *Magma Redox Geochemistry.* 2021. p. 233–53.
62. Neuville DR. Viscosity, structure and mixing in (Ca, Na) silicate melts. *Chem Geol.* 2006;229(1):28–41.
63. Le Losq C, Neuville DR, Florian P, Henderson GS, Massiot D. The role of Al³⁺ on rheology and structural changes in

sodium silicate and aluminosilicate glasses and melts. *Geochim Cosmochim Acta*. 2014;126:495–517.

SUPPORTING INFORMATION

Additional supporting information can be found online in the Supporting Information section at the end of this article.

How to cite this article: Pereira L, Schuller S, Wadsworth FB, Vasseur J, Lancelotti RF, Hess K-U, et al. Rheology of a sodium-molybdenum borosilicate melt undergoing phase separation. *Int J Appl Glass Sci*. 2024;15:127–38.
<https://doi.org/10.1111/ijag.16650>